Journal of Materials Chemistry C

# Enhanced charge mediator properties of photocatalysts with reduced graphene nanoribbons for photocatalytic acceleration of hydrogen production in aqueous media

| | |
|---|---|
| Journal: | *Journal of Materials Chemistry C* |
| Manuscript ID | TC-ART-10-2023-003622.R1 |
| Article Type: | Paper |
| Date Submitted by the Author: | 29-Nov-2023 |
| Complete List of Authors: | Morita, Ryono; Kyushu University Faculty of Engineering Graduate School of Engineering Department of Applied Chemistry<br>Murakami, Yasushi; Kyushu University Faculty of Engineering Graduate School of Engineering Department of Applied Chemistry<br>Shen, Xiao-Feng; Kyushu University, Department of Automotive Science<br>Yang, Dengyao; Kyushu University International Institute for Carbon-neutral Energy Research<br>Watanabe, Motonori; Kyushu University, International Institute for Carbon-Neutral Energy Research<br>Song, Jun Tae; Kyushu University, Applied Chemistry<br>Takagaki, Atsushi; Yokohama National University Graduate School of Engineering,<br>Ishihara, Tatsumi; Kyushu University, Department of Applied chemistry Faculty of Engineering |
| | |

ARTICLE

# Enhanced charge mediator properties of photocatalysts with reduced graphene nanoribbons for photocatalytic acceleration of hydrogen production in aqueous media

Received 00th January 20xx,
Accepted 00th January 20xx

DOI: 10.1039/x0xx00000x

Ryono Morita[a], Yasushi Murakami[a], Xiao Feng Shen[b], Dengyao Yang[b,c], Motonori Watanabe[a,b,c,d*], Jun Tae Song[a,c], Atsushi Takagaki[e] and Tatsumi Ishihara[a,b,c,d]

In this study, a hybrid photocatalyst with titanium oxide using reduced graphene nanoribbons (rGNR) was fabricated. The resulting 0.5wt% platinum-loaded titanium oxide-supported reduced GNR (Pt/$TiO_2$/rGNR) exhibited an activity of 2.54 mmol $h^{-1}$ $g^{-1}$ which is 6.35 times higher than the 0.40 mmol $h^{-1}$ $g^{-1}$ of the titanium oxide photocatalyst. This activity was also higher than that of the starting material, multi-walled carbon nanotube (MWCNT)-supported titanium oxide (Pt/$TiO_2$/MWCNT) as 0.80 mmol $h^{-1}$ $g^{-1}$. The resulting catalysts were characterized by X-ray photoelectron spectroscopy (XPS) and fluorescence lifetime spectroscopy, and the GNRs chemically reduced by $NaBH_4$ (rGNR) had higher conductivity than the GNRs reduced by photogenerated electrons (pGNR) from titanium oxide. The photocatalytic reaction and photocurrent test found that almost no photoresponsivity of reduced GNR character was exhibited. This result clarified that the reduced GNRs played a role as a mediator that promotes charge separation between photocatalysts and that effective hydrogen production in water was achieved.

## Introduction

Environmental changes caused by global warming are due to greenhouse gases such as carbon dioxide ($CO_2$), which are emitted from burning fossil fuels. To reduce $CO_2$ emissions, there is a worldwide need for green energy transmission materials that do not emit $CO_2$. Solar energy is an attractive renewable energy alternative to fossil fuels.[1,2] Converting solar energy into chemical energy is a very useful means of storing solar energy efficiently and as a sustainable energy carrier with minimal environmental impact. Among the solar fuels produced by artificial photosynthesis, hydrogen is expected to be the one of most attractive energy carriers because it can be compressed and transported and does not produce pollutants when burned [3,4]. Hydrogen can be used in highly efficient power generation systems such as internal combustion engines and fuel cells and can be produced electricity from water and sunlight. In addition, hydrogen can be combined with atmospheric carbon dioxide and emissions from coal- and natural gas-fired plants to produce precursors for methanol, synthetic natural gas, plastics, and fertilizers [5]. One of the most important challenges in realizing such a process is efficient and cost-effective water splitting at the scale needed to meet the world's energy needs (i.e., tens of terawatts) [6]. Solar fuel from water splitting using particulate semiconductors as a photocatalyst, both sunlight absorption and catalysis can be performed by a single particle, and the system is a relatively low-cost system in the light-driven photocatalytic system [7, 8]. However, the solar hydrogen production system using the powder has not reached the efficiency required for practical application [9,10]. Therefore, further design and development of efficient photocatalysts is important. To increase the efficiency of water splitting, a photocatalyst can be combined with carbon materials to achieve a charge-separated state [11]. The carbon materials can be chosen such as active carbon [12], fullerene [13], CNT [14], carbon nitride-based materials [15], and graphene-based materials [16-18]. Graphene-based composite photocatalysts are used as a typical example because this 2D structure. This can be enhanced the light-energy adsorption and reaction site due to large surface area, also improvement of the composite charge separation properties due to high conductivity and redox properties. Srivastava et al. reported the enhancement of photocatalytic properties with reduced graphene oxide/$TiO_2$ composite [19]. Kudo et al. demonstrated the Z-scheme type photocatalytic reaction in $BiVO_4$ and $SrTiO_3$ with reduced graphene oxide as a redox mediator [20]. Gopinath et al. reported a film type of photocatalyst with Au/Pd/graphene oxide/$TiO_2$ for hydrogen production [21]. Graphene-based composites were also accepted to use the $CO_2$ reductive conversion photocatalyst [22]. These developments indicated that graphene-based materials showed highly promising

[a] Department of Applied Chemistry, Faculty of Engineering, Kyushu University, 744 Motooka, Nishi-ku, Fukuoka 819-0395, Japan. Email: mwata@i2cner.kyushu-u.ac.jp
[b] Department of Automotive Science, Graduate School of Integrated Frontier Sciences, Kyushu University 744 Motooka, Nishi-ku, Fukuoka 819-0395, Japan.
[c] International Institute for Carbon-Neutral Energy Research (WPI-I2CNER), Kyushu University, 744 Motooka, Nishi-ku, Fukuoka 819-0395, Japan.
[d] Center for Energy Systems Design (CESD), Kyushu University, 744 Motooka, Nishi-ku, Fukuoka 819-0395, Japan
[e] Division of Materials and Chemical Engineering, Faculty of Engineering, Yokohama National University, 79-5 Tokiwadai, Hodogaya-ku, Yokohama, 240-8501, Japan

Electronic Supplementary Information (ESI) available: XPS spectra of Mn 2p for GNR, photocurrent test of GNR, XPS spectra of relative peak proportions, XRD and SEM data of after photocatalytic reaction, and Summary of related Pt/$TiO_2$/carbon materials composites photocatalytic activities. See DOI: 10.1039/x0xx00000x

composites for photocatalytic reactions. One of the disadvantages of graphene-based composites was the difficulty of fabrication with the non-oxidized structure of graphene due to the low dispersibility in aqueous solution because of its hydrophobicity. To overcome this issue, graphene oxide can be used for photocatalytic reactions, however low crystallinity and difficulty in controlling charge traps make reducing of the photocatalytic activity [23,24]. Tour et al. reported the top-down synthesized graphene nanoribbon (GNR) from CNT has higher crystallinity and conductivity than graphene oxide, and is expected as a new charge transfer material [25]. It was demonstrated that GNR can be used in such supercapacitors [26,27], transistors [28], and aerogel for conductive materials [29] suggesting high conductive and redox mediator properties. Recently, Liu et al. reported that CdS/GNR obtained by oxidative cleavage of carbon nanotubes into graphene nanoribbons followed by supporting cadmium sulfide showed high photocatalytic hydrogen production performance. [30] Serge Ayissi et al., estimated that anatase or rutile phase of $TiO_2$ and graphene nanoribbons can be electro chemical interaction at chemisorption sites of graphene structure.[31] Zhizhong Han et al., reported that graphene nanoribbon decorated $TiO_2$ nanosheet enhanced photocatalytic organic dye decomposition property than that of $TiO_2$ nanosheet itself. [32] H. Esmaili et al., reported that photo-electrochemical water splitting with naphthalene diimide functionalized graphene nanoribbons as water oxidation layer on $TiO_2$ film. [33] These results strongly suggested that the interaction of $TiO_2$ and graphene nanoribbons can be enhanced photocatalytic activity due to effective charge separation between interfaces of graphene/$TiO_2$ surfaces. However, photocatalytic nanoribbons generally used in oxide state, which has many oxygen-derived modification groups exist on the surface of GNRs obtained by oxidative cleavage and function as electron trapping sites. Such modification sites can be removed by reductive techniques such as hydrogen reduction treatment and hydrazine chemical reduction [25]. Here, we reported the synthesis, structural, physical, and photocatalytic properties of the anatase $TiO_2$ nanoparticle loaded GNR by sol-gel hydrothermal method. By oxidative cleavage of MWCNT, oxidative GNR was synthesized. Two different methods of loading platinum co-catalysts on $TiO_2$/GNR were investigated. One is the reduction of platinum by photoexcited electrons supplied by titanium dioxide and the other is the chemical reduction of $NaBH_4$. These reduction methods not only supported platinum on $TiO_2$/GNR but also reduced the excessively oxidized GNR skeleton. In particular, the oxidized GNR skeleton reduced by $NaBH_4$ acted as an effective charge transport medium and greatly improved the photocatalytic activity.

## Experimental

### General

X-ray diffraction (XRD) patterns were collected on an X'Pert Pro PANalytical diffractometer with Cu Kα radiation (λ = 0.15418 nm). Transmission electron microscopy (TEM) was performed on a JEOL JEM ARM200F microscope (200 kV). X-ray photoelectron spectroscopy (XPS) was measured with Kratos Ultra2. IR spectra were measured with Shimadzu IR Prestige-21. Raman spectra were tested with Renishaw inVia Raman Microscopes. The UV−visible diffuse reflectance (UV−vis DR) spectra were recorded using a UV−vis spectrometer (HITACHI U-3310) equipped with an integrating sphere. Photoluminescence (PL) spectra were measured using a HITACHI F-7000 instrument with an excitation wavelength of 265 nm. The PL decay was determined using a HORIBA Jobin Yvon FluoroHub with a TBX-PS detector source. A HORIBA 265 nm NanoLED (<1.2 154 ns pulse) was used for the excitation. Particle size distribution was corrected with a Horiba LA-920 analyzer. Photocurrent tests potentials were measured with a BAS-100B/W electrochemical analyzer, measurements were performed using a cell equipped with catalysts-loaded FTO glass as the working electrode, a platinum wire as the counter electrode, and Ag/AgCl as the reference electrode. Impedance tests were performed Ivium CompactStat.h system.

### Preparation of photocatalysts

### Preparation of Pt/$TiO_2$

$TiO_2$ was prepared using the sol-gel method [34]. Titanium tetra isopropoxide (Wako 1.63 g) was added to ethanol (150 mL) and titrated with a mixture of ethanol (Nacalai Tesque, 99%) and acetic acid (Nacalai Tesque, containing 99% acetic acid, 30 mL/30 mL) for 1 hour while stirring. The pH was then adjusted to pH=9 with ammonia water (Nacalai Tesque, containing 28% ammonia), followed by suction filtration, washing with ion exchange water, drying at 60 °C, and calcination at 300 °C for 30 minutes. Pt/$TiO_2$ was prepared by the reduction of $H_2PtCl_6$ (Sigma-Aldrich, 8 wt% in $H_2O$) to the prepared $TiO_2$ by $NaBH_4$ (Nacalai Tesque, 92%) aqueous solution. Synthesized $TiO_2$ (100.0 mg) was dispersed in ion exchange water (10 mL), to which $H_2PtCl_6$ (12.5 μL) and $NaBH_4$ (1M, 1 mL) were added in one portion, stirred for 30 minutes, suction filtered, washed with ion exchange water, and dried at 60 °C.

### Preparation of Pt/$TiO_2$/MWCNT

Pt/$TiO_2$/MWCNT was synthesized as follows. MWCNT (150.0 mg) was well dispersed in EtOH (150 mL) by ultrasonication. Titanium tetra isopropoxide (Wako, 1.63 g) was dropped into MWCNT-containing solution, followed by AcOH/EtOH (30 mL/30 mL) for 60 minutes at 25 °C. The suspended solution was adjusted to pH = 9 by ammonia water solution (28%). The reactant of MWCNT was filtered through a membrane filter (ADVANTEC, pore size:0.5 μm), and washed with DI water. The filtrate was calcined for 30 minutes. at 300 °C to give MWCNT/GNR (450.0 mg).

### Preparation of $TiO_2$/GNR

Graphene nanoribbon (GNR) was synthesized according to the literature [25]. Briefly, MWCNT (Sigma-Aldrich, >95 %, 50-90 nm diameter, 500.0 mg) was portioned once into concentrated $H_2SO_4$ (Nacalai Tesque, 97%, 100mL) and $KMnO_4$ (Nacalai Tesque, 1.5 g, 99.3%) for 30 minutes [25, 32]. at 25 °C. After the reaction, the suspended solution was suction filtered through a membrane filter (ADVANTEC, pore size: 0.5 μm), washed with concentrated HCl (Nacalai Tesque, 35%), followed by DI water. The GNR (800.0 mg) was given after drying at 50 °C. GNR (150.0 mg) was well dispersed in EtOH (150 mL) by ultrasonication. Titanium tetra isopropoxide (Wako, 1.63 g) was added into GNR solution, followed by AcOH/EtOH (30mL/30 mL) for 60 minutes at 25 °C. The suspended solution was adjusted to pH = 9 by an aqueous $NH_3$ solution (28%). The reactant of GNR was corrected through a membrane filter (ADVANTEC, pore

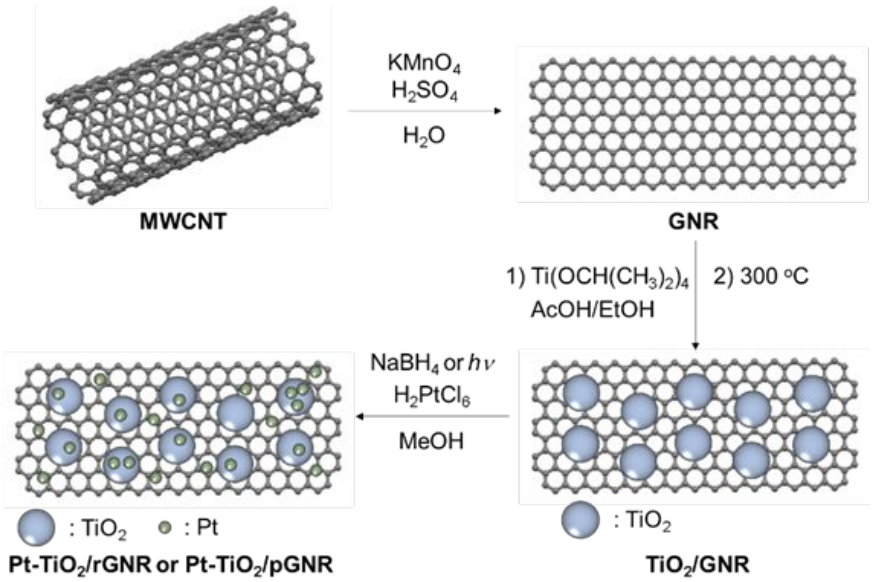


**Figure 1. Synthetic procedure of Pt/$TiO_2$/rGNR or Pt/$TiO_2$/pGNR composite**

size:0.5 μm), and washed DI water. The filtrate was calcined for 30 minutes at 300 °C to give $TiO_2$/GNR (450.0 mg).

**Pt/$TiO_2$/rGNR (reduced GNR: Pt loading by $NaBH_4$ with chemical reduction of GNR)**

$H_2PtCl_6$ (Sigma-Aldrich, 8 wt% in $H_2O$, 12.5 μL) was added into GNR suspense solution, followed by rapidly injected $NaBH_4$ aqueous solution (1M, 1 mL) at 25 °C. After 30 minutes, the reactant of $TiO_2$/rGNR was filtered through a membrane filter (ADVANTEC, pore size:0.5 μm), and washed with DI water. The Pt/$TiO_2$/rGNR (800.0 mg) was given after drying at 50 °C.

**Pt/$TiO_2$/pGNR (pGNR: Pt loading by photo deposition method with photochemical reducing GNR)**

$H_2PtCl_6$ (Sigma-Aldrich, 8 wt% in $H_2O$, 12.5 μL) was added into GNR suspense solution, followed by rapidly injected $NaBH_4$ aqueous solution (1M, 1 mL) at 25 °C. After 30 minutes, the reactant of $TiO_2$/GNR was filtered through a membrane filter (ADVANTEC, pore size:0.5 μm), and washed with DI water. The Pt/$TiO_2$/GNR (800.0 mg) was given after drying at 50 °C.

**Photocatalytic reaction**

The photocatalytic water splitting was performed using a closed gas circulating glass reactor with a dead volume of 350 $cm^3$. The photocatalyst (50 mg) was dispersed in a quartz reaction cell including 10 mM MeOH/distilled water (30 mL). The atmosphere of the reaction cell was exchanged to Ar (100 Torr). The reaction cell was irradiated using a 300 W Xe lamp (Cermax PE300BUV, Excelitas Technologies Corp.) under magnetic stirring. The light intensity of the Xe lamp was adjusted to 1.3 W $cm^{-2}$. The evolved gases were detected using a gas chromatograph (GC 8A, Shimadzu Corp.) equipped with a thermal conductivity detector.

## Results and discussion

The synthetic procedure of the Pt/$TiO_2$/GNR composite was illustrated in Figure 1. MWCNT was unzipped to be suspended in a $KMnO_4$/concentrated $H_2SO_4$ solution. Synthesized GNR was loaded with $TiO_2$ nanoparticles by sol-gel condensation method. Finally, metallic platinum as a co-catalyst was loaded by in-situ $Pt^0$ generation with $H_2PtCl_6$ as a precursor and $NaBH_4$ reduction reagent. At this time, the GNR of some oxidized groups was reduced to generate a reduced-GNR structure (rGNR: GNRs chemically reduced with $NaBH_4$.). We also performed photoreduction using excited titanium oxide. In this case, the electrons generated by titanium oxide not only reduced the platinum species, but also reduced of some oxidized species to the photo-reduced GNRs structure (pGNR: GNRs reduced by photogenerated electrons from photo excited $TiO_2$). The structures of GNR and Pt/$TiO_2$ supported on the catalyst were analyzed by several techniques including XRD, IR, Raman, UV–vis DR, XPS, and TEM. Figure 2a showed the XRD pattern of starting material MWCNT, synthesized GNR, Pt/$TiO_2$, Pt/$TiO_2$/MWCNT, Pt/$TiO_2$/pGNR and Pt/$TiO_2$/rGNR. After the oxidation of MWCNT, a characteristic peak of MWCNT at 26.4° disappeared while the pattern of GNR showed at 9.9°, 26.1°, and 42.8°. These peaks pattern is in good agreement with the reports from other group [25]; thus, it was confirmed that the MWCNT-unzipped structure of GNR was synthesized. Pt/$TiO_2$ was synthesized by sol-gel method and then platinum-loaded with $NaBH_4$ reduction of $H_2PtCl_6$. The diffraction peak pattern of 25.2°, 38.5°, 48.2°, 58.9°, 63.1°, 69.4°, and 75.4° was assigned to the anatase phase (JCPDS Card no. 21-1272). No platinum peak was observed, suggesting small nano-particle platinum was supported. When Pt/$TiO_2$/MWCNT was fabricated by the above method in the presence of MWCNT, the $TiO_2$ anatase phase at 25.2°, 38.5°, 48.2°, 58.9°, 63.1°, 69.4°, and 75.4° and the peak of MWCNT at 26.2° could be observed. On the other hand, Pt/$TiO_2$/rGNR showed peaks around 25.2° and 42.7°, while a characteristic peak in GNR at 9.9°disappeared. The peak at 9.9° in

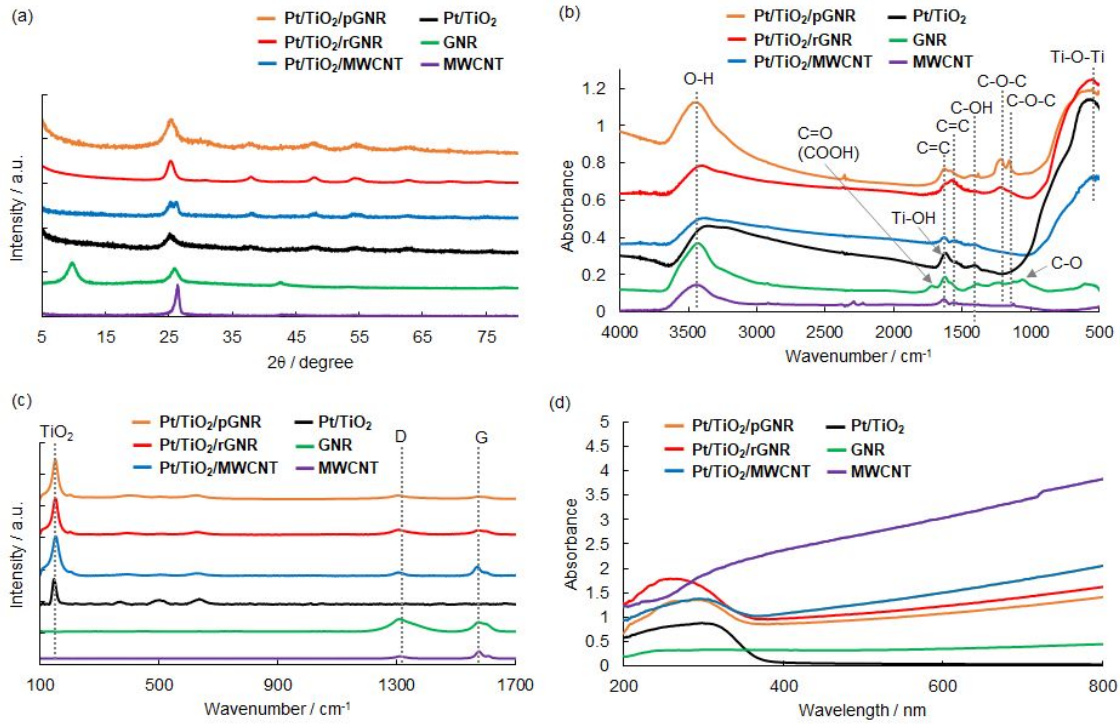


Figure 2. Characterization of MWCNT, GNR, Pt/$TiO_2$, and after Pt/$TiO_2$ loaded samples. (a) XRD patterns, (b) IR spectra (c) Raman spectra, and (d) DRS spectra.

GNR is due to intercalation of oxygen-containing functional groups[35], which moved the (001) peak to a lower diffraction angle; for Pt/$TiO_2$/rGNR and Pt/$TiO_2$/pGNR after hydride reduction with $NaBH_4$ and photoreduction reaction, the (001) peak moved to a higher diffraction angle in the Pt/$TiO_2$/rGNR and Pt/$TiO_2$/pGNR. The shorter interlayer distance of the GNR materials after reduction may be due to the significant removal of oxygen-containing functional groups. [36] IR spectrum of MWCNT showed adsorbed $H_2O$ of -OH stretching peak at 3410, 1617 $cm^{-1}$ and CNT skeleton of C=C peaks at 1617 (overlapped with -OH stretching peak) and 1574 $cm^{-1}$ (Figure 2(b))[37]. Unzipped structure of GNR from MWCNT showed new peaks at 1716 $cm^{-1}$ for C=O stretching mode, 1627 and 1567 $cm^{-1}$ for C=C stretching mode, and 1396 $cm^{-1}$ for C-OH stretching mode, and 1204 and 1153 $cm^{-1}$ for C-O-C stretching mode, and 1063 $cm^{-1}$ for C-O stretching mode [38]. $TiO_2$ showed water adsorption peaks at 3380 and 1618 $cm^{-1}$, and characteristic Ti-O-Ti bond at 572 $cm^{-1}$ [39]. Pt/$TiO_2$/MWCNT, Pt/$TiO_2$/rGNR, and Pt/$TiO_2$/pGNR have confirmed the peaks of adsorbed water of -OH stretching peak at around 3380, 1618 $cm^{-1}$ and additional peaks of Ti-O-Ti at 572 $cm^{-1}$. In the case of Pt/$TiO_2$/rGNR and Pt/$TiO_2$/pGNR, the peaks of C=O and C-O almost disappeared, while C=C, -OH, and C-O-C peaks remained. This fact suggested that $NaBH_4$ of hydride nor $TiO_2$ photo excited driven electrons acted as a reducing agent and reduced the carboxyl and C–O groups of the GNR structure. (Figure 2(b)). Raman measurements were performed to further investigate the condition of the composite and the defect structure of the carbon material (Figure 2(c)). MWCNT showed typical G and D bands at 1577 $cm^{-1}$ and 1311 $cm^{-1}$, respectively with G/D = 1.76 ratio. GNR of G/D ratio showed 0.37, suggesting the surface of GNR has oxidized defect sites such as COOH, OH, and C-O-C, as IR spectra confirmed. After loading Pt/$TiO_2$ on the carbon materials, similar G/D ratio of 1.79 with the anatase phase of $TiO_2$ at 638, 502, 382, and 147 $cm^{-1}$ was observed for Pt/$TiO_2$/MWCNT, indicating no change in the CNT surface. Pt/$TiO_2$/rGNR showed a higher G/D ratio of 0.67 than GNR of 0.37, supporting the results of reduction of surface defect sites such as C=O and C-O-C groups as seen in IR measurements. Pt/$TiO_2$/pGNR of G/D ratio of 0.58 was lower than Pt/$TiO_2$/rGNR, suggesting that in the $NaBH_4$ reduction process, more GNR defect structures are converted to graphene structures than photoreduction process. Diffuse reflectance spectra of MWCNT showed wide-range adsorption at 200-800 nm (Figure 2(d))[40]. After the unzipped structure of GNR, around 300-800 nm of absorption was weaker due to $sp_2$ conjugation being terminated. In the Pt/$TiO_2$, a characteristic band at 200-380 nm was observed, and these peaks were also confirmed in the Pt/$TiO_2$/MWCNT, Pt/$TiO_2$/pGNR, and Pt/$TiO_2$/rGNR. The band gap of the $TiO_2$ in these materials is the same as 3.26 eV. In the Pt/$TiO_2$/pGNR, and the Pt/$TiO_2$/rGNR of absorption spectra, 400-800 nm of intensities were increased composition with GNR. Tour et al. have reported that hydrazine treatment reduces the oxidized sites on the surface of nanoribbons grown from MWCNTs, expanding the π-conjugated system and causing an absorption shift toward longer wavelengths [25]. The formation of new absorption bands in GNRs is explained by the broadening of the conjugated system due to the reduction of nanoribbons by electrons generated by $NaBH_4$ reduction or photoexcitation. Further surface information of materials was conducted with XPS (Figure 3). The GNRs did not observe any Mn peaks, confirming that there is no Mn doping in the GNRs due to $KMnO_4$ treatment (Fig S1). In the C 1s spectra, MWCNT

showed C-C/C=C bonds (284.3 eV), C-OH bonds (285.6 eV), and π–π* bonds (291.0 eV), while GNR showed new components as C-O/O-C-O bonds (286.4 eV), C=O (287.9 eV), and O-C=O bonds (288.9 eV)[41]. In O 1s spectra, MWCNT showed almost no peaks, while GNR showed new peaks for C-OH bonds (533.1 eV), for C-O bonds (532.2 eV), and C=O bonds (531.2 eV). C 1s and O 1s spectra results suggested the surface of GNR containing the oxidized OH and COOH moiety [42]. After loading the Pt-$TiO_2$ on the carbon materials, MWCNT showed O 1s spectra of Ti-O bonds at 530.6 eV and Ti 2p spectra of Ti 2p3/2 at 459.1 eV, suggesting the surface located the $TiO_2$.

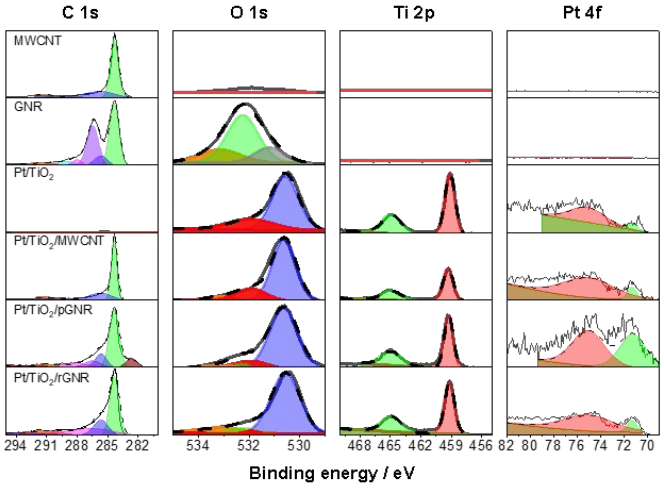


Figure 3. XPS spectra of MWCNT, GNR, Pt/$TiO_2$, Pt/$TiO_2$/MWCNT, Pt/$TiO_2$/pGNR and Pt/$TiO_2$/rGNR.

Pt/$TiO_2$/rGNR also successively confirmed Ti-O bond and Ti 2p3/2, while all of the Pt-loaded materials confirmed Pt 4f spectra, suggested Pt was located on the surface of Pt/$TiO_2$, Pt/$TiO_2$/MWCNT, and Pt/$TiO_2$/GNR materials. In the Pt/$TiO_2$/pGNR and the Pt/$TiO_2$/rGNR spectra, disappearing/decreasing of the C 1s spectra components of C=O (287.9 eV), and O-C=O bonds (288.9 eV), and O1s spectra components of C-O (533.1 eV), C-O (532.2 eV), and (531.1 eV) were found. These tendencies were consistent with IR spectra. The detail of the relative peak proportions for XPS analysis were summarized in Tables S1-S3.

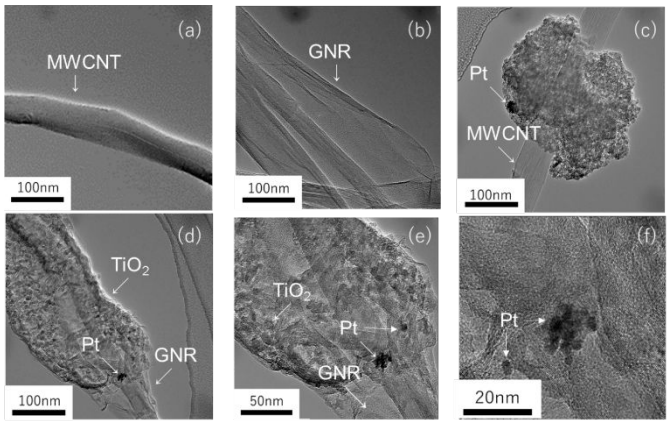


Figure 4. TEM images of (a) MWCNT, (b) GNR (c) Pt/$TiO_2$/MWCNT and (d-f) Pt/$TiO_2$/rGNR composite.

To insight into the morphology of Pt/$TiO_2$ on carbon material, a TEM image was measured. Figures 4(a-b) showed MWCNT and GNR for this study used. Around 50 nm diameter of MWCNT was unzipped, and 200-250 nm width of GNR was confirmed. Figures 4(c-d) showed TEM images of MWCNT and GNR after Pt/$TiO_2$ loading. After Pt/$TiO_2$ was loaded with MWCNT, it was confirmed that $TiO_2$ was aggregated and supported on the surface of MWCNT in a branched form. In the case of GNR, titanium oxide was widely supported on the surface of GNR. The MWCNT had a Brunauer–Emmett–Teller (BET) surface area of 25.0 $m^2g^{-1}$ and the GNR had a surface area of 69.8 $m^2g^{-1}$. The large surface area of GNR is considered to contribute to the dispersion support of titanium oxide uniformly. Pt nanoparticles less than 5 nm in size were found in both Pt/$TiO_2$/MWCNT and Pt/$TiO_2$/GNR composites. After Pt/$TiO_2$ loaded composites of surfaces area was 182.4 $m^2g^{-1}$ for Pt/$TiO_2$/MWCNT and 190.2 $m^2g^{-1}$ for Pt/$TiO_2$/GNR. In the control experiment, the sol-gel method synthesized Pt/$TiO_2$ without carbon materials of the surface area showed 183.4 $m^2g^{-1}$ which was in good agreement with reported the material obtained by the similar synthetic method for 197 $m^2g^{-1}$ [34]. The value of Pt/$TiO_2$ was similar to Pt/$TiO_2$/MWCNT and Pt/$TiO_2$/GNR composites, indicating that $TiO_2$ was successfully deposited on the carbon materials in a similar manner. The BET surface areas were summarised in Table S4.

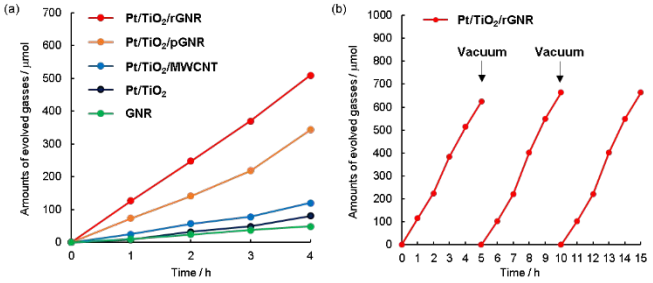


Figure 5. Photocatalytic hydrogen production over Pt/$TiO_2$/carbon materials composites in 10 mM MeOH/$H_2O$.

The water splitting reaction under light irradiation was performed by a 300-W Xenon lamp. As shown in Figure 5a, Pt/$TiO_2$ showed the $H_2$ formation rates as 20 μmol/h. In the Pt/$TiO_2$ and carbon material composites, Pt/$TiO_2$/rGNR and Pt/$TiO_2$/pGNR showed higher $H_2$ formation rates of 127 μmol/h and 73 μmol/h than Pt/$TiO_2$/MWCNT catalyst showed 40 μmol/h. Furthermore, Pt/rGNR obtained by $NaBH_4$ reduction and heat treatment without adding titanium oxide process showed a hydrogen production rate of 18 μmol/h, suggesting that synthesized GNR itself of photocatalytic property is insufficient. This result shows that GNR acts as a charge mediator rather than as a photocatalyst. To confirm the stability of Pt/$TiO_2$/GNR, photocatalytic hydrogen production was three times repeated. In Figure 5b, during three times of hydrogen production, no decrease in the hydrogen production rate was observed. After photoreaction of XRD patterns of photocatalysts did not show no change the peak and any characteristic Pt peaks were observed (Figure S3), and SEM-EDX measurements also confirmed no growth of Pt peaks after photoreaction (Figures S4-7). These results

suggested that photocatalysts were stable and Pt was no aggregated during photocatalytic reaction. The apparent quantum efficiency (AQY) showed 9.5% for 350 nm, while no hydrogen production was observed in the range of 450 nm and 500 nm. The fact that the region showing photocatalytic activity in the Pt/$TiO_2$/GNR system is the ultraviolet region is due to the reason that the titanium oxide portion of this catalytic system is photoexcited to promote the photocatalytic reaction. In Table S5, the platinum-supported system showed higher AQY compared to similar studies on titanium oxide/graphene systems [43-53]. Compared with CdS/GNR [30], it showed a comparable hydrogen generation rate. Our results showed that reducing graphene showed high activity, indicating that GNRs also act as electron mediators that facilitate charge transfer by performing reduction treatment.

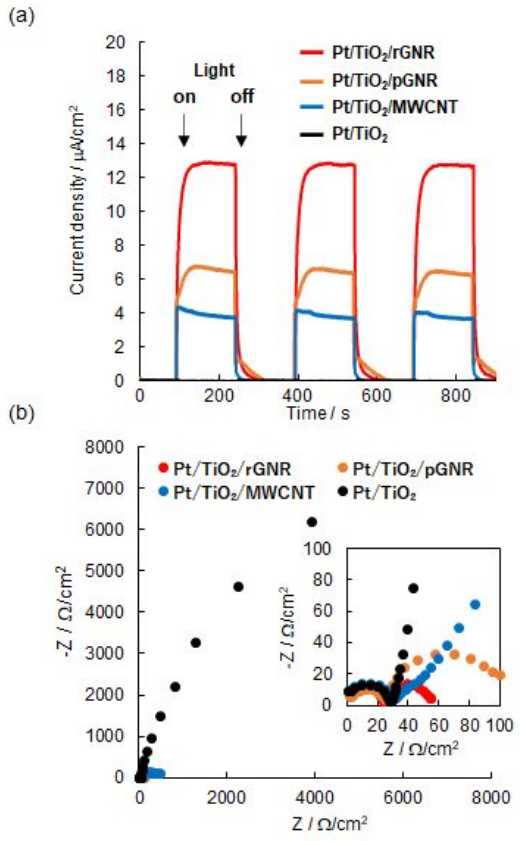


Figure 6. Pt/$TiO_2$ and Pt/$TiO_2$/carbon composites on FTO glass for (a) photocurrent measurement and (b) impedance spectra.

Under the same condition to the photocatalytic hydrogen production reaction, photocurrent was measured. In Figure 6(a), under the chopped illumination, the photocurrent density was found in the following order: Pt/$TiO_2$/rGNR > Pt/$TiO_2$/pGNR >Pt/$TiO_2$/MWCNT > Pt/$TiO_2$. The Pt/$TiO_2$ showed photocatalytic activity under chopping irradiation, however, a small photocurrent density was observed. On the other hand, high photocurrent density in Pt-$TiO_2$/GNRs was observed, indicating an increased electron transport in Pt-$TiO_2$/GNRs system. The photocurrent of the reduced GNR (rGNR) that was prepared by $NaBH_4$ treatment is similar to that of GNR, suggesting that the rGNR in this study is low photo-responsibility (Figure S2). The Pt/$TiO_2$/rGNR and Pt/$TiO_2$/pGNR showed higher photocurrent than the Pt/$TiO_2$/MWCNT; this suggests that effective charge transport occurs between the $TiO_2$ photocatalyst on reduced GNR materials. In the impedance spectra (0.1 – 10 MHz) showed two semi-circles, where contact resistance between the electrode and current collector (Rs) and the charge-transfer resistance (Rct) of electrode materials. Pt/$TiO_2$ shows high resistance for Rs = 14.1 Ω $cm^{-2}$ and Rct = 4028.4 Ω $cm^{-2}$. The pGNR showed a smaller resistance for Rs = 10.7 Ω $cm^{-2}$ and Rct = 31.3 Ω $cm^{-2}$, indicating that the GNR act as the electron mediator. Thus Pt/$TiO_2$/rGNR showed more smaller resistance Rs = 10.6 Ω $cm^{-2}$ and Rct = 12.2 Ω $cm^{-2}$ than pGNR. It is considered that this is because Pt/$TiO_2$/rGNR has higher conductivity. After all, the structure of GNR is reduced by $NaBH_4$ reduction creating a structure with fewer defect sites.

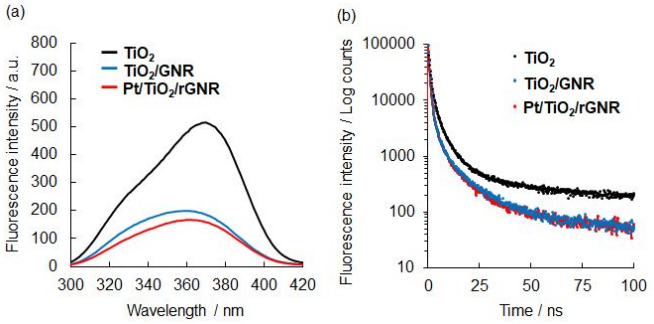


Figure 7. (a) Fluorescence spectra and (b) fluorescence decay spectra of $TiO_2$, $TiO_2$/GNR, and Pt/$TiO_2$/rGNR.

The photocatalytic reaction mechanism of Pt/$TiO_2$/GNR was a further consideration. Figure 7a shows fluorescence (FL) spectra of photocatalysts tested. The spectral features of $TiO_2$ and $TiO_2$/rGNR are similar, implying that no new emission is generated from rGNR or $TiO_2$/rGNR composites. The FL intensity of $TiO_2$/rGNR is smaller than that of $TiO_2$. This indicates that rGNR can rapidly accept electrons generated by photoexcitation of $TiO_2$ and effectively inhibit electron-hole recombination. Pt/$TiO_2$/rGNR with platinum supported further decreases, meaning that the platinum receives electrons from titanium oxide and rGNR, promoting the more effective charge separation state. Figure 7b shows the fluorescence decay plots of $TiO_2$, $TiO_2$/GNR, and Pt/$TiO_2$/rGNR.

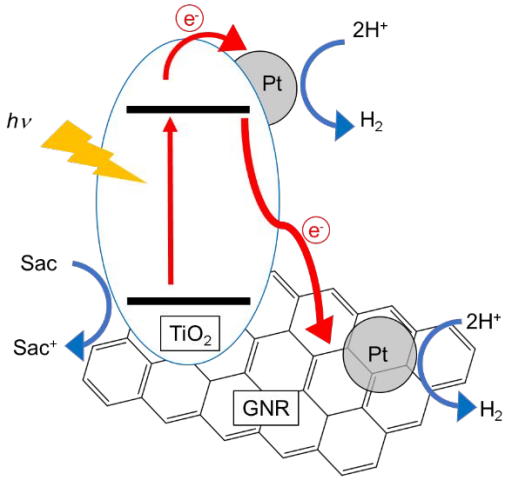

Figure 8. Proposed mechanism of photocatalytic hydrogen production in $Pt/TiO_2$/rGNR system.

The fluorescence lifetimes of $TiO_2$, $TiO_2$/GNR, and $Pt/TiO_2$/rGNR excited at 295 nm showed $\tau_1$, $\tau_2$ = 1.94 ns, 12.1 ns, $\tau_1$, $\tau_2$ = 1.07 ns, 9.40 ns, and $\tau_1$, $\tau_2$ = 1.03 ns, 8.41 ns, respectively. In the case of graphene oxide–$TiO_2$ composites study, effective charge separation shows decreasing in the fluorescence and fluorescence decay lifetime [54, 55]. These results suggested that the charge was separated between GNR, $TiO_2$, and Pt and that the charge transfer from $TiO_2$ to Pt via GNR was expected. Based on the above experimental results, Figure 8 is a proposed hydrogen production mechanism by the photocatalyst. Photoexcited titanium oxide charge-separates electrons into conduction band (CB) and holes into valence band (VB) of titanium oxide. Electrons collected on the CB are injected into the GNR. The highly conductive GNRs with their oxidative modification sites removed either chemical reduction from $NaBH_4$ or by photoexcited electrons supplied from titanium oxide efficiently charge to separate the electrons from the platinum and transfer the electrons to the platinum near the titanium oxide or the platinum on the GNRs. As a result, electrons react with protons on platinum to produce hydrogen. At this time, the holes remaining in the VB of the titanium oxide disappear as electrons are supplied from the sacrificial agent, methanol. GNRs act as high charge-transfer sites, resulting in enhanced photocatalytic activity compared to $TiO_2$ alone.

## Conclusions

GNRs were prepared from MWCNTs by oxidative cleavage, and photocatalytic hydrogen production reactions in water were investigated using composite materials of reduced GNRs, which were chemically or photogenerated electron-reduced, and titanium oxide. GNRs obtained from MWCNTs had carboxy groups, C-O-C, and CO substituents. These substituents disappeared in rGNR obtained by $NaBH_4$ reduction except for C-O-C. On the other hand, in pGNR using photogenerated electrons from titanium oxide, C=O remains in addition to C-O-C, and these results were supported by IR, Raman, and XPS spectroscopy. The resulting $Pt/TiO_2$/rGNR and $Pt/TiO_2$/pGNR exhibited an activity of 2.54 and 1.46 mmol $h^{-1}g^{-1}$ which is higher than the 0.40 mmol $h^{-1}g^{-1}$ of the $Pt/TiO_2$ photocatalyst. This activity was also higher than that of the starting material, $Pt/TiO_2$/MWCNT as 0.80 mmol $h^{-1}g^{-1}$. $Pt/TiO_2$/rGNR showed 9.5% in 350 nm UV light, showing higher AQY activity than previously reported titanium oxide/carbon composites. Photocatalytic experiments and photocurrent measurements showed that GNRs have almost no photo response, and impedance measurements showed that GNRs have high conductivity. Therefore, GNR has the role of electron mediator between $TiO_2$ and platinum. These results report the properties of reduced GNRs in photocatalytic reactions and may pave the way for future applications of reduced GNRs in related studies.

## Author Contributions

Conceptualization: Ryono Morita, Motonori Watanabe; Methodology: Ryono Morita, Motonori Watanabe; Formal analysis and investigation: Ryono Morita, Yasushi Murakami, Xiao Feng Shen, Dengyao Yang; Writing - original draft preparation: Ryono Morita, Motonori Watanabe, Jun Tae Song, Atsushi Takagaki, Tatsumi Ishihara; Funding acquisition: Motonori Watanabe, Tatsumi Ishihara; Resources: Motonori Watanabe, Tatsumi Ishihara; Supervision: Motonori Watanabe

## Conflicts of interest

There are no conflicts to declare.

## Acknowledgements

This study was supported by the Grant-in-Aids for Science Research (21K04692) from the Ministry of Education, Culture, Sports, Science, and Technology (MEXT, Japan), and the Strategic International Collaborative Research Program (SICORP) concerning “Research on Hydrogen as a renewable energy carrier’’ from the Japan Science and Technology Agency (JST). X.F.S. acknowledges the support by JST, the establishment of university fellowships towards the creation of science technology innovation, Grant Number JPMJFS2132. M.W. and T. I. acknowledges the support from I2CNER and Center for Energy Systems Design (CESD), funded by the World Premier International Research Center Initiative (WPI), MEXT, Japan.

## Notes and references

[1] Y. Tachibana, L. Vayssieres, J. R. Durrant, Nat. Photonics, 2012, 6, 511–518.
[2]M. A. Green, S. P. Bremner, Nat. Mater., 2016, 16, 23–34.
[3]K. Mazloomi, C. Gomes, Renew. Sustain. Energy Rev., 2012, 16, 3024–3033.
[4] S.-S. Zhu,, Y. Liu, X.-L. Chen, L.-B. Qu, B. Yu, ACS Catal., 2021, 12, 126–134.
[5] Z. W. Seh, J. Kibsgaard, C. F Dickens, I. Chorkendorff, J. K Nørskov, T. F Jaramillo, Science, 2017, 355, 146.
[6] N. S. Lewis, Science, 2016, 351, aad1920.
[7] B. A. Pinaud, J. D. Benck, L. C. Seitz, A. J. Forman, Z. Chen, T. G. Deutsch, B. D. James, K. N. Baum, G. N. Baum, S. Ardo, H. Wang, E. Millere T. F. Jaramillo, Energy Environ. Sci., 2013, 6, 1983–2002.
[8] L. S.F. Frowijn, W. G.J.H.M. SarkSustainable, Energy Technol. Assess., 2021, 48, 101631.
[9] H. Nishiyama, T. Yamada, M. Nakabayashi, Y. Maehara, M. Yamaguchi, Y. Kuromiya, Y. Nagatsuma, H. Tokudome, S. Akiyama, T. Watanabe, R. Narushima, S. Okunaka, N. Shibata, T. Takata, T. Hisatomi, K. Domen, Nature, 2021, 598, 304–307.
[10] S. Chen, T. Takata, K. Domen, Nature Rev. Materials, 2017, 2, 17050.
[11] S. Cao, J. Yu, J. Photochem. Photobiol. C, 2016, 27, 72-99.
[12] M. Hakamizadeh, S. Afshar, A. Tadjarodi, R. Khajavian, M. R. Fadaie, B. Bozorgi, Int. J. Hydro. Energy, 2014, 39, 7262-7269.
[13] Z. C. Lian, P. P. Xu, W. C. Wang, D. Q. Zhang, S. N. Xiao, X. Li and G. S. Li, ACS Appl. Mater. Interfaces, 2015, 7, 4533–4540.
[14] J. Zhang, M. Dai, S. Zhang, M. Dai, P. Zhang, S. Wang, Z. He, Solar RRL, 2022, 6, 2200243.
[15] L. Zhou, H. Zhang, H. Sun, S. Liu, M. O. Tade, S. Wang, W. Jinc, Catal. Sci. Technol., 2016, 6, 7002-7023.
[16] K.-Q. Lu, Y.-H. Li, Z.-R. Tang, Y.-J. Xu, ACS Mater. Au, 2021, 1, 37–54.
[17] S. Mishra, R. Acharya, Mater. Today: Proceedings, 2021, 35, 164-169.
[18] M. A. Ahmed, A. A. Mohamed, RSC Adv., 2023, 13, 421-439.
[19] P. K. Dubey, P. Tripathi, R.S. Tiwari, A.S.K. Sinha, O.N. Srivastava, Int. J. Hydro. Energy, 2014, 39, 16282-16292.
[20] A. Iwase, S. Yoshino, T. Takayama, Y. H. Ng, R. Amal, A. Kudo, J. Am. Chem. Soc., 2016, 138, 10260‑10264.

[21] B. Tudu, N. Nalajala, K. P. Reddy, P. Saikia, C. S. Gopinath, ACS Appl. Mater. Interfaces, 2019, 11, 32869–32878.
[22] M.-Q. Yang, Y.-J. Xu, Nanoscale Horiz., 2016, 1, 185-200.
[23] I. A. Kotin, I. V. Antonova, O. M. Orlov, S. A. Smagulova, Mater. Res. Express, 2016, 3, 066301.
[24] P. N. O. Gillespie, N. Martsinovich, ACS Appl. Mater. Interfaces, 2019, 11, 31909–31922.
[25] D. V. Kosynkin, A. L. Higginbotham, A. Sinitskii, J. R. Lomeda, A. Dimiev, B. K. Price, J. M. Tour, Nature, 2009, 458, 872–876.
[26] W. Ma, W. Li, M. Li, Q. Mao, Z. Pan, J. Hu, X. Li, M. Zhu, Y. Zhang, Adv. Funct. Mater., 2021, 31, 2100195.
[27] M. Saghafi, F. Mahboubi, S. Mohajerzadeh, M. Fathi, R. Holze, Curr. Appl. Phys., 2014, 14, 1335-1343.
[28] H. Tanaka, R. Arima, M. Fukumori, D. Tanaka, R. Negishi, Y. Kobayashi, S. Kasai, T. K. Yamada, T. Ogawa, Sci. Rep., 2015, 5, 12341.
[29] Q. Peng, Y. Li, X. He, X. Gui, Y. Shang, C. Wang, C. Wang, W. Zhao, S. Du, E. Shi, P. Li, D. Wu, A. Cao, Adv. Mater., 2014, 26, 3241-3247.
[30] Y. Xia , B. Cheng, J. Fan, J. Yu, G. Liu, Small, 2019, 15, 1902459.
[31] S. Ayissi, P.A. Charpentier, N. Farhangi, J.A. Wood, K. Palotas, W.A. Hofer, J. Phys. Chem. C, 2013, 117, 25424-25432.
[32] Z. Han, L. Wei, H. Pan, C. Li, J. Chen, J. Mol. Catal. A Chem., 2015, 398, 399-406
[33] H. Esmaili, E. Kowsari, S. Ramakrishna, A. Motamedisade, G.G. Andersson, Mater. Today Chem., 2022, 24, 100900.
[34] Z. Li, B. Gao, G. Zheng Chen, R. Mokaya, S. Sotiropoulos, G. L, Puma, Appl. Catal. B, 2011, 110, 50-57.
[35] H.-H. Huang, K. Kanishka, H. De Silva, G. R. A. Kumara, M. Yoshimura, Sci. Rep., 2018, 8, 6849.
[36] K.-H. Hung, C.-H. Chan, H.-W. Wang, Renew. Energy, 2014, 66, 150-158.
[37] J. H. Lehman, M. Terrones, E. Mansfield, K. E. Hurst, V. Meunier, Carbon, 2011, 49, 2581-2602.
[38] K. Krishnamoorthy, M. Veerapandian, K. Yun, S.-J. Kim, Carbon, 2013, 53, 38-49
[39] J. He, D. Chen, Y. Li, J. Shao, J. Xie, Y. Sun, Z. Yan, J. Wang, Appl. Phys. A, 2013, 113, 327–332.
[40] Y.-J. Xu, Y. Zhuang, X. Fu, J. Phys. Chem. C, 2010, 114, 2669–676.
[41] Y. Zhang, G. Liu, S. Yu, J. Zhang, Y. Tang, P. Li, Y. Ren, ACS Appl. Mater. Interfaces, 2014, 6, 20968–20977.
[42] R. Al-Gaashani A. Najjar, Y. Zakaria, S. Mansour, M.A. Atieh, Ceram. Int., 2019, 45, 14439-14448.
[43] X.-Y. Zhang, H.-P. Li, X.-L. Cui, Y. Lin, J. Mater. Chem., 2010, 20, 2801–2806.
[44] H. Kim, G. Moon, D. Monllor-Satoca, Y. Park, W. Choi, J. Phys. Chem. C, 2012, 116, 1535–1543.
[45] P. Zeng, Q. Zhang, X. Zhang, T. Peng, J. Alloys Comp., 2012, 516, 85-90.
[46] Z. Mou, Y. Wu, J. Sun, P. Yang, Y. Du, C. Lu, ACS Appl. Mater. Interfaces, 2014, 6, 13798−13806.
[47] R. O. da Silva, F. J. Heiligtag, M. Karnahl, H. Junge, M. Niederberger, S. Wohlrab, Catal. Today, 2015, 246, 101-107.
[48] Y. Zhu, Y. Wang, W. Yao, R. Zonga, Y. Zhu, RSC Adv., 2015, 5, 29201–29208.
[49] L. Li, L. Yu, Z. Lin, G. Yang, ACS Appl. Mater. Interfaces, 2016, 8, 8536−8545.
[50] Y. Shinde, S. Wadhai, A. Ponkshe, S. Kapoor, P. Thakur, Int. J. Hydro. Energy, 2018, 43, 4015-4027.
[51] S. Mohan P, M. K. Purkait, C.-T. Chang, Int. J. Hydro. Energy, 2020, 45, 17174-17190.
[52] H. E. Marouazi, P. Jiménez-Calvo, E. Breniaux, C. Colbeau-Justin, I. Janowska, V. Keller, ACS Sustainable Chem. Eng., 2021, 9, 3633–3646.
[53] A. Pollap, J. Serafin, I. Serrano, J. Srenscek-Nazzal, J. Llorca, J. Environ. Chem. Engineer., 2022, 10, 108877.
[54] R. Sellappan, J. Sun, A. Galeckas, N. Lindvall, A. Yurgens, A. Y. Kuznetsov, D. Chakarov, Phys. Chem. Chem. Phys., 2013, 15, 15528-15537.
[55] K. Zhou, Y. Zhu, X. Yang, X. Jiang, C. Li, New J. Chem., 2011, 35, 353-359.